Chemistry–A European Journal
Research Article
doi.org/10.1002/chem.202104420
Chemistry Europe
European Chemical Societies Publishing
www.chemeurj.org

Anticancer Aminoferrocene Derivatives Inducing Production of Mitochondrial Reactive Oxygen Species

Hülya Gizem Özkan,[a] Vanrajsinh Thakor,[a] Hong-Gui Xu,[a] Galyna Bila,[b] Rostyslav Bilyy,[b] Daria Bida,[a] Martin Böttcher,[c] Dimitrios Mougiakakos,[c] Rainer Tietze,[d] and Andriy Mokhir*[a]

Abstract: Elevated levels of reactive oxygen species (ROS) and deficient mitochondria are two weak points of cancer cells. Their simultaneous targeting is a valid therapeutic strategy to design highly potent anticancer drugs. The remaining challenge is to limit the drug effects to cancer cells without affecting normal ones. We have previously developed three aminoferrocene (AF)-based derivatives, which are activated in the presence of elevated levels of ROS present in cancer cells with formation of electron-rich compounds able to generate ROS and reduce mitochondrial membrane potential (MMP). All of them exhibit important drawbacks including either low efficacy or high unspecific toxicity that prevents their application in vivo up to date. Herein we describe unusual AF-derivatives lacking these drawbacks. These compounds act via an alternative mechanism: they are chemically stable in the presence of ROS, generate mitochondrial ROS in cancer cells, but not normal cells and exhibit anticancer effect in vivo.

Introduction

A common consequence of transformation of normal to cancer cells is altered homeostasis of reactive oxygen species (ROS). The transformed cells steadily produce ROS leading to their elevated intracellular level. Furthermore, cancer cells are more sensitive to exogenous ROS than normal cells.[1] As a consequence, drugs producing ROS can exhibit anticancer effects.[1] Since ROS are highly cytotoxic, the challenge in the therapeutic application of such drugs is to achieve cancer cell specificity to avoid expected detrimental effects on normal cells and tissues. To address this issue, we have introduced cancer specific aminoferrocene (AF)-based ROS amplifiers (type A agents„ Figure 1A, the activation is triggered by B–C oxidation).[2] Other known drugs/agents activated in the presence of ROS and amplifying ROS in cells include procarbazine (HN-NH oxidation),[3] hydroxyferrocifenes (C–H oxidation)[4] and organochalcogenides (RXR oxidation, where X=Se or Te).[5]

Activation of the AF-agents starts with spontaneous hydrolysis of the boronic acid pinacol ester moiety (agents **1a**–**6a**, Figure 1A) with formation of boronic acid derivatives (drugs **1b**–**6b**). These further react with ROS, triggering the reaction sequence that leads to formation of AF Fc–NH–R'. The activation occurs only in ROS-rich (cancer) cells. Redox potentials of Fc–NH–R' products are shifted −300 to −400 mV with respect to the parent agents. These electron rich catalyst are capable of donating an electron to hydrogen peroxide (H_2O_2) thereby transforming this less reactive ROS to highly reactive and toxic hydroxyl radicals ($HO^{\bullet}$).[2] The latter species can be detected in cytoplasm by using 5(6)-chloromethyl-2',7'-dichlorodihydro-fluorescein diacetate (CM-DCFH-DA). Since the intracellular localization of CM-DCFH-DA is not biased, it senses ROS in the whole cell. In this paper we call the CM-DCFH-DA-sensitive intracellular pool of ROS total ROS or tROS. Both previously developed AF derivatives **2a**[6] and **3a**,[7] exhibiting anticancer effects in vivo, were found to strongly induce tROS generation. In contrast, they either do not or weakly affect mitochondrial ROS (mROS), detected by using MitoSOX™ probe.

Apart from the elevated ROS, mitochondria functions in transformed cells are partially impaired. Therefore, glycolysis is switched from oxidative phosphorylation, which is typical for normal cells, to anaerobic metabolism.[8] However, these cells still rely on remaining mitochondrial functions, including, for example, triphosphate and nucleotide synthesis.[9] Correspond-

[a] H. Gizem Özkan, V. Thakor, H.-G. Xu, D. Bida, Prof. Dr. A. Mokhir
Department of Chemistry and Pharmacy
Friedrich-Alexander-University of Erlangen Nuremberg (FAU)
Organic Chemistry II, 91058 Erlangen (Germany)
E-mail: Andriy.Mokhir@fau.de
[b] G. Bila, Prof. Dr. R. Bilyy
Danylo Halytsky Lviv National Medical University
Pekarska str. 69, 79010 Lviv (Ukraine)
[c] Dr. M. Böttcher, Prof. Dr. D. Mougiakakos
Department of Otorhinolaryngology
Otto-von-Guericke-University of Magdeburg, Medicinal Faculty, University Hospital for Hematology and Oncology
Leipzigerstraße 44, 39120 Magdeburg (Germany)
[d] Dr. R. Tietze
Department of Otorhinolaryngology, Head and Neck Surgery, Section of Experimental Oncology and Nanomedicine (SEON)
Friedrich-Alexander-University of Erlangen Nuremberg (FAU), University Hospital
Glückstraße 10a, 91054 Erlangen (Germany)

Supporting information for this article is available on the WWW under https://doi.org/10.1002/chem.202104420

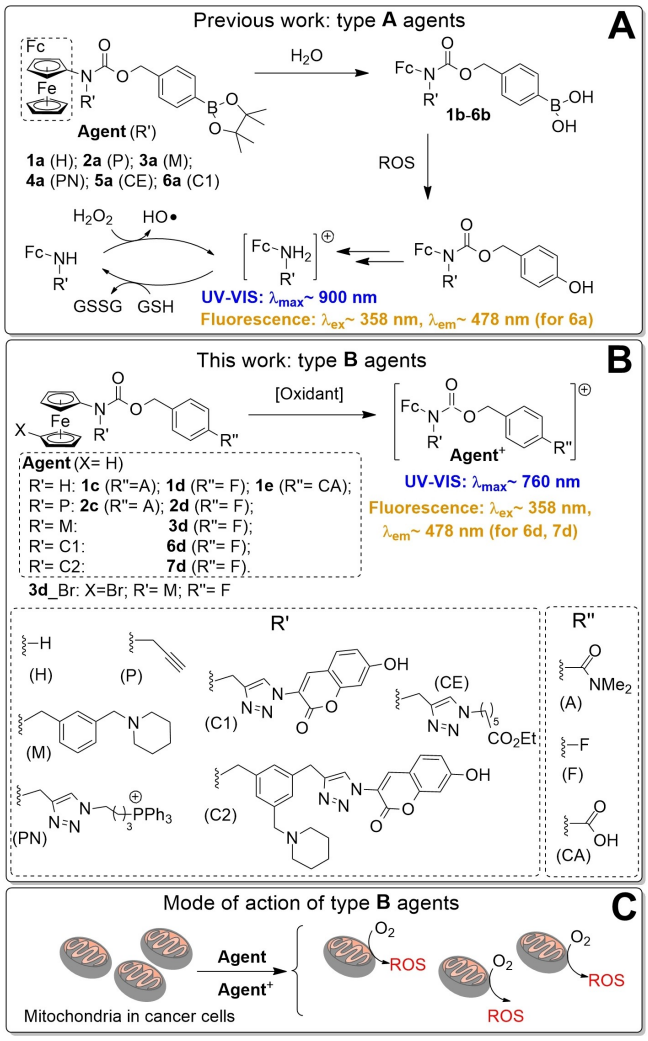

Figure 1. A: Structure and the mechanism of activation of previously known type **A** agents. **B**: Structures of type **B** agents and their oxidized form. **C**: A cartoon illustrating generation of mitochondrial ROS (mROS) by type **B** agents. [Oxidant]: intracellular oxidants, for example ROS, peroxidases.

ingly, targeting mitochondria is a viable strategy for anticancer therapy. Based on these considerations, it would be interesting to develop AF drugs able to amplify ROS in proximity to mitochondria (mROS). That would affect mitochondrial function and increase the intracellular ROS level, thereby targeting simultaneously two weak points of cancer cells.

Previously, we have described two ROS-amplifying AF agents **4a**[10] and **5a**,[11] which affect mitochondria in different human cancer cell lines (Figure 1). These agents exhibit important drawbacks precluding their further development. In particular, **4a** is highly toxic to normal cells, whereas **5a** is taken up by cancer cells poorly leading to its low anticancer efficacy. We have also reported on endoplasmic reticulum (ER)-targeting AF drugs, which generate mROS in human cancer cells.[12] However, they exhibit substantial unspecific toxicity that precludes in vivo applications at therapeutically active doses. The observed problems with mROS-generating AF drugs are not surprising. Normal cells are highly sensitive to mROS, since they support stress signaling and induce mutations in mitochondrial and genomic DNAs thereby promoting neoplastic transformation.[13] Therefore, the cancer vs. normal cell specificity for mROS-generating agents should be especially high to be able to achieve useful therapeutic effects.

We have serendipitously discovered that AF derivatives, in which a ROS-sensitive moiety is replaced with a ROS-resistant fragment (R''=F, type B agents, Figure 1B), generate mROS in cancer cells, whereas normal cells remain unaffected. In this paper, we report on detailed studies of these new agents as well as their close analogues including their synthesis, characterization and basic properties. We studied the mechanism of action of type B agents and evaluated their anticancer efficacies in vitro (on selected cancer cell lines and primary cells) and in vivo (murine Nemeth-Kellner lymphoma, NK/Ly).

Results and Discussion

Reference compounds **1a**–**5a** were prepared as previously reported.[2,6,7,11,12] Compounds **1c**–**1e**, **2c**, **2d**, **3d**, their brominated (**3d**_Br, Figure 1B) and fluorogenic (**6d**, **7d**) analogues as well as control **6a** were prepared as described in detail in the Supporting Information. All new compounds were >95% pure according to C, H, N analysis. Their solubility in phosphate-buffered saline (PBS, pH 7.4) exceeded 25 μM and in Roswell Park Memorial Institute (RPMI) medium containing 5% of fetal bovine serum (FBS) - 100 μM (Table S1, Supporting Information).

Preliminary studies

Type A agents (e.g. **1a**–**6a**) lose the pinacol fragment in aqueous neutral solutions within <2 h forming boronic acids (**1b**–**6b**). As previously reported,[14] the latter species are responsible for the anticancer activity of these agents. In this work, we used ROS-resistant N,N-dimethylaminocarbonyl (A) analogues as negative controls since the polarity of the A fragment matches that of the boronic acid fragment. The latter is confirmed by similar n-octanol/water partition coefficients (logP's) of the following pairs of agents and controls: logP(**1b**) = 2.76 ± 0.23 vs. logP(**1c**) = 3.36 ± 0.11 and logP(**2b**) = 3.35 ± 0.25 vs. logP(**2c**) = 3.96 ± 0.15 (Table 1). Based on these data, it is expected that passive cellular uptake of the agents and the controls is comparable to each other. Therefore, differences in their activity should not be related to different uptake efficacies. In contrast to **1a** and **2a**, negative controls **1c** ($E_{1/2}$ = −70 mV vs. FcH) and **2c** ($E_{1/2}$ = −10 mV vs. FcH) cannot be transformed via route *I* to the electron rich Fc–NH–R' products ($E_{1/2}$ = −300 to −400 mV vs. FcH, Figure 1A). Correspondingly, they (a) are poor catalysts for ROS generation in cell free settings with the efficacies slightly higher than those of ferrocene (FcH, Table 1), (b) induce production of less tROS in representative human cancer ovarian (A2780) cells and (c) are less toxic to A2780 cells than the corresponding drugs **1a** and **2a** (Table 1). In despite of this expected trend, we were puzzled by the fact that both **1c**

Table 1. Comparison of selected properties of type **A** and **B** agents.

Agent	LogP[a]	$E_{1/2}$[b]	ROS releasing efficacy[c]	IC_{50} [μM][d] A2780 cells	BL-2 cells
1a	5.00 ± 0.30	−70	57 ± 7	23.9 ± 2.7	35.5 ± 2.5
1b	2.76 ± 0.23	–	–	–	–
1c	3.36 ± 0.11	−70	6 ± 1	46.1 ± 8.5	–
1d	4.17 ± 0.27	−76	7 ± 1	15.0 ± 2.4	17.9 ± 4.8
1e	1.90 ± 0.04	−70	8 ± 1	> 50	–
2a	5.51 ± 0.17	−10	54 ± 7	14.2 ± 2.1	20.1 ± 0.9
2b	3.35 ± 0.25	–	–	–	–
2c	3.96 ± 0.15	−10	2.5 ± 0.7	37.1 ± 6.2	–
2d	4.72 ± 0.15	−15	1.1 ± 0.3	16.7 ± 2.5	18.2 ± 1.6
3a	> 6.26	−40	54 ± 6	5.6 ± 1.7	3.9 ± 0.3
3b	6.09 ± 0.03	–	–	–	–
3c	5.79 ± 0.03	−35	5 ± 1	–	–
3d	6.05 ± 0.07	−35	2.7 ± 0.8	7.0 ± 1.3	3.3 ± 0.3
3d_Br	6.22 ± 0.07	116	4.3 ± 0.9	6.2 ± 0.1	–
FcH	3.40	0	0.4 ± 0.2	> 50	> 50

[a] LogP: n-octanol/water partition coefficients. [b] $E_{1/2}$: redox potentials *versus* ferrocene/ferrocenium redox couple (FcH/FcH^+) in mV. [c] ROS releasing efficacy is expressed as the maximal increase of the fluorescence intensity of 2′,7′-dichlorofluorescin in the presence drugs/controls ($(dF/dt)_0$, min^{-1}, F: λ_{ex} = 501 nm; λ_{em} = 525 nm). The increase of $(dF/dt)_0$ for the background (N,N-dimethylformamide (DMF, 1 %, v/v) in 3-(N-morpholino)propanesulfonic acid buffer (MOPS buffer, 100 mM, pH 7.4) containing N,N,N′,N′-ethylenediaminetetraacetic acid (EDTA, 10 mM), glutathione (GSH, 5 mM) and H_2O_2 (10 mM)) was 0.3 ± 0.1. [d] IC_{50}: a concentration, at which half of the cells remain viable; A2780: human ovarian cancer cells; BL-2: human Burkitt's lymphoma cells.

and **2c** increase the level of tROS in A2780 cells to some degree (**1c** by 2.2 ± 0.6; **2c** by 6.1 ± 0.7 fold as compared to the effect of the carrier only (DMSO)) and exhibit the moderate anticancer activity. In contrast, ferrocene, which has similar to **1c** and **2c** redox potential (Table 1), is not toxic under these conditions. The mechanism of the ROS production by **1c** and **2c** is not related to that of the previously known AF agents. In the following sections of this paper we will use term "type B" for the new agents originally derived from negative controls **1c** and **2c** with R′ = A, F and CA (Figure 1).

Optimization of the anticancer activity of type B agents

With the goal to understand the effect of lipophilicity on the anticancer activity of type B agents, we prepared two analogues of **1c** containing fluorine (**1d**) and a carboxylic acid residue (**1e**) in place of the "A" fragment. **1d** is more (logP = 4.17 ± 0.27) and **1e** (logP = 1.90 ± 0.04) – less lipophilic than **1c**. Redox potentials as well as ROS releasing ability in cell free settings of all these compounds are practically identical (Table 1). We found that the cytotoxicity towards A2780 cells in this small series correlates with lipophilicity (Table 1). To further optimize most active **1d**, we introduced at its carbamate nitrogen either propargyl (P) or 3-(N-piperidinomethyl)benzyl (M) fragments to obtain **2d** and **3d**, correspondingly. Though **2d** is slightly more lipophilic than **1d**, it does not lead to the higher cytotoxicity towards A2780 cells. In contrast, substantially more lipophilic **3d** (**3d**: logP = 6.05 ± 0.07) exhibits the highest activity among all new drugs reported in this paper: IC_{50}(**3d**) = 7.0 ± 1.3 μM (Table 1). The effect is not only restricted to one cell line. In particular, **3d** is active against Burkitt's lymphoma BL-2 cells (IC_{50}(**3d**) = 3.3 ± 0.3 μM, Table 1) as well as primary chronic lymphocytic leukemia (CLL) cells (IC_{50}(**3d**) = 4.8 ± 2.0 μM, Figure 2).

The efficacy of **3d** against all studied cells (A2780, BL-2 and CLL cells) was found to be the same as that of the corresponding type A agent **3a** (Table 1, Figure 2, Student's t test).

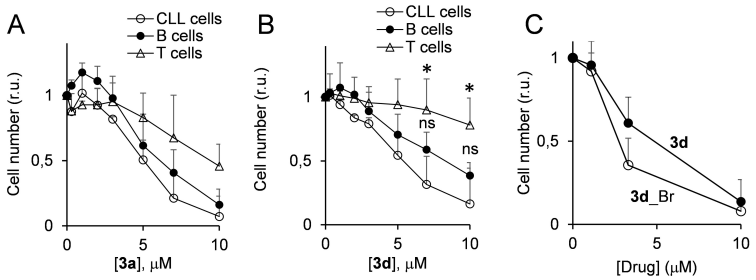

Figure 2. Effect of agents **3a** (inset **A**) and **3d** (inset **B**) on viability of primary cancer and normal cells (CLL, B and T cells). **C**: Effects of **3d** and **3d** < **?** > Br on viability of CLL cells. Student's t test: * - $p < 0.05$, ns – non-significant, $p \geq 0.05$.

A mechanism of uptake and anticancer activity of agent 3 d

First, we investigated the uptake of **3 d** and known agent **3 a** by A2780 cells by monitoring the increase of iron amount ($[Iron]_i$) in the cells treated with the drugs (Figure 3A). To determine the mechanism of this process, we conducted the experiment at 37 and 4 °C (Figure 3A). At 37 °C the uptake of both agents was the same and strong, whereas at 4 °C it was significantly inhibited for **3 a**, but not affected for **3 d**. These data indicate different uptake mechanisms of the agents. For **3 a** it is at least partially energy dependent (active or facilitated) and for **3 d** – energy independent (passive).

Furthermore, we found that analogously to **3 a** agent **3 d** induces the statistically significant increase of tROS in A2780 cells. However, the effect of **3 d** is substantially weaker than that of **3 a** ($p < 0.05$, Student's t test, Figure 3B). Interestingly, the low tROS generated in **3 d**-treated cells is still important for the anticancer activity of the agent. This is confirmed by the concentration dependent attenuation of cytotoxicity of **3 d** in the presence of the ROS scavenger N-acetyl cysteine (NAC, Figure 3C). As expected, the same effect is also observed for **3 a**. Despite **3 d** produces the lower amount of tROS in cells, it exhibits the same anticancer efficacy as the potent ROS generator **3 a**. These data indicate that, additionally to tROS, **3 d** might induce another intracellular toxicity factor. We found that this factor is mROS. In particular, the level of mROS (detected by using a MitoSOX™ probe) in A2780 cells treated either with the carrier or type A agent **3 a** for 2 h is very low as indicated by the weak red signal in fluorescence images E and I (Figure 3). Nuclei of the cells were counter-stained with a dye Hoechst 33342 (blue color) that was used as a reference signal for comparing changes in the intensity of the red fluorescence between different samples. In contrast to the control probes, the level of mROS in the **3 d**-treated cells is substantially higher as indicated by the intense red signal in image M. These qualitative microscopic data were fully confirmed by the accurate quantification of the intracellular mROS level using flow cytometry (Figure 3P). Since **3 d** itself is not a ROS amplifier (in contrast to **3 a**) as confirmed by the ROS-release experiment in cell free setting (Table 1), mROS should be generated indirectly. To get a hint on how this can happen, we investigated effects of **3 d** on mitochondria and lysosomes of cancer cells. Mitochondria were selected, since drug-induced disturbance of their function can lead to the inefficient electron transfer causing the electron leakage and formation of mROS. Lysosomes were selected, since **3 d** could be accumulated in these organelles due to the presence of a piperidine moiety (a lysosomal carrier) in its structure. By using mitochondrial membrane potential (MMP) sensitive probe rhodamine 123 (R123), we found that both **3 d** and **3 a** strongly reduce MMP in A2780 cells, whereas **2 a** is also active, but less efficient (Figure 4A). The effect of both type A agents **2 a** and **3 a** is saturated after 2 h incubation, whereas type B agent **3 d** is acting slower. In particular, the MMP of A2780 cells is decreased stronger after 4 h than after 2 h incubation with **3 d** ($p < 0.01$, Student's t test). These data indicate that mROS generated by

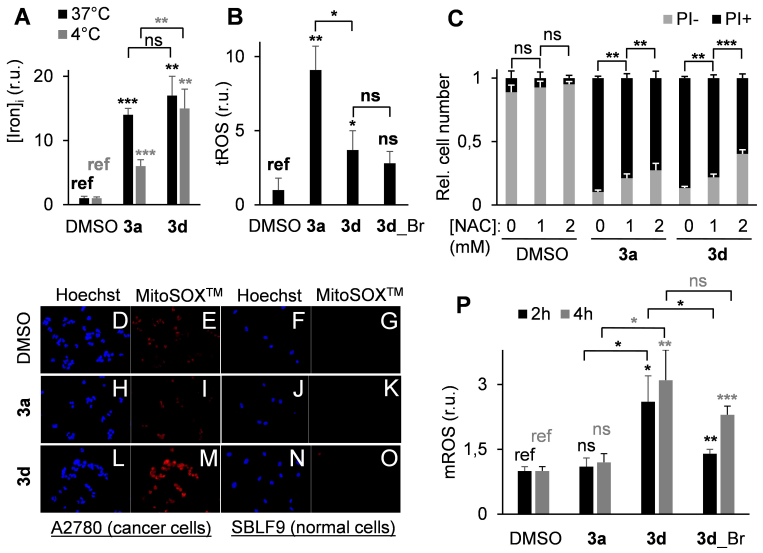

Figure 3. Uptake efficacy and involvement of ROS in the anticancer effect of agent **3 d** and Ref. [**3 a**]. **A**: The efficacy of uptake of **3 a** and **3 d** by A2780 cells at 37 °C (black bars) and 4 °C (grey bars), determined by monitoring the increase of the intracellular iron concentration ($[Iron]_i$). **B**: Increase of tROS (responsive to a CM-DCFH-DA probe) in A2780 cells in the presence of **3 a** and **3 d** (each 25 μM, 2 h incubation), monitored by using flow cytometry: $\lambda_{ex} = 488$ nm; $\lambda_{em} = 475$–565 nm. The amount of tROS obtained for the "DMSO"-sample was used as a reference and set to "1". The level of tROS for all other samples is indicated in relative units (r.u.). **C**: Effects of N-acetylcystein (NAC: 1 and 2 mM) on cytotoxicity of a carrier (DMSO), **3 a** and **3 d** (20 μM). PI = propidium iodide. Live cells are indicated "PI−". Dead (necrotic) cells are indicated "PI+". The sum of "PI−" and "PI+" cells for each sample was set to "1". The relative numbers of "PI−" and "PI+" cells are plotted on the OY axis. **D**–**O**: Effect of **3 a** and **3 d** (each 25 μM, 2 h incubation) on mROS in A2780 and SBLF9 cells, monitored by fluorescence microscopy: Hoechst (blue color) – $\lambda_{ex} = 365$ nm; $\lambda_{em} = 395$–495 nm (detection of nuclei by using Hoechst 33342 as a probe); MitoSOX™ (red color) – $\lambda_{ex} = 538$–562 nm; $\lambda_{em} = 570$–640 nm. **P**: Increase of mROS (responsive to a MitoSOX™ probe) in A2780 cells in the presence of **3 a** and **3 d** (each 25 μM, incubation: 2 h (black bars), 4 h (grey bars)), monitored by using flow cytometry: $\lambda_{ex} = 488$ nm; λ_{em}: 543–627 nm. Student's t test: * – $p < 0.05$; ** – $p < 0.01$; *** – $p < 0.001$; ns – non-significant, $p \geq 0.05$. Ref: references (color coded), against which Student's test was applied.

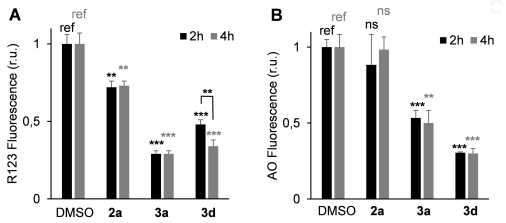

Figure 4. Effect of a carrier (DMSO), agents **2a**, **3a** and **3d** (each 25 μM, incubation time: 1 h (black bars) and 2 h (grey bars)) on mitochondrial membrane potential (MMP, probe: R123, inset A) and the lysosome-specific fluorescence (probe acridine orange (AO), inset B). Monitoring by flow cytometry: for R123 – λ_{ex} = 488 nm; λ_{em} = 475–565 nm; for AO – λ_{ex} = 365 nm; λ_{em} = 645–745 nm. Student's t test: ** – $p < 0.01$; *** – $p < 0.001$; ns – non-significant, $p \geq 0.05$. Ref: references (color coded), against which Student's test was applied.

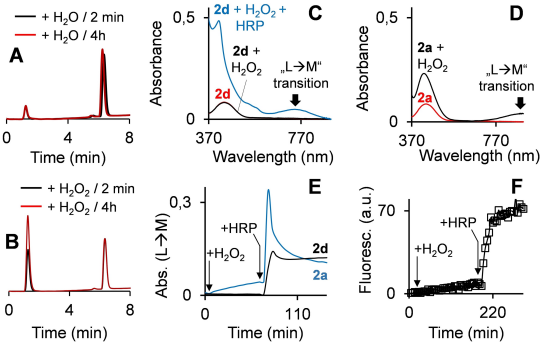

Figure 5. A, **B**: HPLC analysis of solutions of **3d** (100 μM) dissolved in a mixture of DMSO (1%, v/v) in aqueous phosphate buffer (10 mM, pH 7.4) containing NaCl (150 mM) and GSH (5 mM). The solutions were incubated for 2 min and 4 h in the absence (**A**) and presence of H_2O_2 (**B**, 10 mM) before the analysis. **C**: UV-visible spectra of solutions of **2d** (red trace), **2d** incubated with H_2O_2 for 1 h (black trace), **2d** incubated with H_2O_2 and horseradish peroxidase (HRP) for 1 h (blue trace). "L→M": ligand to metal. **D**: UV-visible spectra of solutions of **2a** (red trace) and **2a** incubated with H_2O_2 for 1 h (black trace). **E**: Dependence of the intensity of "L→M" transitions from time in UV-visible spectra of solutions of **2d** (λ_{max} = 760 nm) and **2a** (λ_{max} = 900 nm). At the time points indicated by arrows H_2O_2 and HRP were added. Other conditions for **C**, **D** and **E**: solvent - methanol/PBS buffer (pH 7.4), 5/3.5, v/v; [drug] = 560 μM; [H_2O_2] = 10 ± 1 mM; [HRP] = 110 ± 30 nM. **F**: Dependence of the fluorescence intensity (λ_{ex} = 358 nm, λ_{em} = 478 nm) from time of the solution of **7d** (20 μM) in acetonitrile/PBS buffer (pH 7.4), 10/79, v/v. At the time points indicated by arrows H_2O_2 (10 ± 1 mM) and HRP (110 ± 30 nM) were added. The initial fluorescence intensity is equal to 0.5 ± 0 a.u. (arbitrary units). The end fluorescence intensity is equal to 71 ± 3 a.u.

3d can be caused by **3d**-induced reduction of MMP in cancer cells.

Further, we found that agent **3d** quenches the fluorescence of A2780 cells loaded with lysosome-specific probe acridine orange (AO). In contrast to the MMP, this effect is saturated already after 2 h incubation. These data might indicate that **3d** is first accumulated in lysosomes before affecting the MMP. As previously reported[7] **3a** also affects the fluorescence of the AO-loaded cells, whereas **2a** lacking in its structure the piperidine moiety (lysosomal carrier) is not active.

Intracellular species responsible for the anticancer effect of 3d

To clarify, which intracellular species **3d** or **3d**$^+$ are responsible for the anticancer activity, we conducted a series of experiments in cell free settings and in cells.

Type B agent **3d** is slightly more electron rich than unmodified ferrocene FcH: $E_{1/2}$ (*versus* FcH/FcH$^+$) = −35 mV. Accordingly, it catalyzes transformation of H_2O_2 to HO$^\bullet$ 6.8-fold more efficiently than FcH (Table 1). In this reaction **3d** donates an electron to H_2O_2 forming **3d**$^+$ at least in catalytic amounts. However, in HPLC of the mixture of **3d** (100 μM) and H_2O_2 (10 mM) we observed only the peak corresponding to **3d**. More polar **3d**$^+$, which was expected to elute at the shorter incubation, was not detected (Figure 5A, B). An analogous type B agent **2d** is more electron rich than **3d**: $E_{1/2}$ (*versus* FcH/FcH$^+$) = −70 mV. However, it is also not oxidized in the presence of H_2O_2 as it is evidenced from both HPLC (data not shown) and UV-visible spectroscopy: the absence of a typical for ferrocenium broad absorbance band at ~600–900 nm corresponding to the ligand-to-metal ("L→M") transition (Figure 5C, E).[15] In another control experiment conducted under the same conditions, the "L→M" transition band at ~900 nm was observed in the spectrum of the mixture of type A agent **2a** (560 μM) and H_2O_2 (10 mM) (Figure 5D). The intensity of this band steadily grows for over 50 min after addition of H_2O_2 to the solution of **2a** (Figure 5E). The latter behavior was expected based on the previously reported mechanism of **2a** activation by ROS via route *I* (Figure 1A). We further found that oxidation of type B agents is possible in the presence of a mixture of H_2O_2 and horseradish peroxidase (HRP), which is a stronger oxidant than H_2O_2 alone. This is indicated by the appearance of the "L→M" transition band in the UV-visible spectrum of the solution containing **2d**, H_2O_2 and HRP (Figure 5C). **2d**$^+$ is formed almost instantaneously after the HRP addition **2d** and H_2O_2 (Figure 5E).

For the study of possible oxidation of type B agents in live cells we prepared a fluorogenic analogue of **3d** containing a 7-hydroxycoumarine dye – **7d**. As controls we also prepared **6d**, which is lacking a piperidine moiety (a fluorogenic version of **2d**), and **6a** (a representative fluorogenic type A agent). These compounds are practically not fluorescent due to the efficient photoinduced electron transfer (PET) from the ferrocenyl moiety to the excited state of the dye. Upon oxidation to the ferrocenium species, the fluorescence of **6a** (via route *I*), **6d** and **7d** (both via route *II*) is increased since PET becomes impossible. The experimental data illustrating this behavior for drug **7d** are provided in Figure 5F. Similarly to its analogue **3d**, drug **7d** is practically not responsive to H_2O_2, whereas it is efficiently oxidized by a mixture of H_2O_2 and HRP that leads to the strong and quick increase of the fluorescence intensity.

By using fluorescence microscopy, we found that A2780 cells loaded with **7d** exhibit weak, but significant fluorescence, whose intensity is not increased by the treatment of the cells with H_2O_2 (Figure 6A–C). In contrast, **6d**-loaded A2780 cells were found to be non-fluorescent. However, by using flow cytometry, which is a more sensitive method, we observed that both **6d**- and **7d**-loaded A2780 and BL-2 cells fluoresce

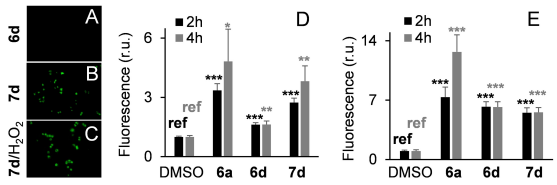

Figure 6. A–C: Fluorescence images (λ_{ex} = 335–383 nm; λ_{em} = 420–470 nm) of A2780 cells incubated with fluorogenic agents **6 d** (inset **A**), **7 d** (inset **B**) and **7 d** followed by H_2O_2 (inset **C**). [Drugs] = 25 μM; [H_2O_2] = 10 mM. The cells were first incubated with the agents for 2 h, washed and incubation for further 1 h with H_2O_2. **D**: Monitoring uptake/activation of **6 a**, **6 d** (both 25 μM) and **7 d** (1 μM) in A2780 (inset **D**) and BL-2 cells (inset **E**) by using flow cytometry: detection at λ_{ex} = 405 nm; λ_{em} = 405–495 nm. Student's t test: * – $p < 0.05$; ** – $p < 0.01$; *** – $p < 0.001$; ns – non-significant, $p \geq 0.05$. Ref: references (color coded), against which Student's test was applied.

significantly stronger ($p < 0.01$ or less, Student's t test) than the cells treated with DMSO only (Figure 6D, E). These data indicate that at least some **6 d**$^+$ and **7 d**$^+$ are formed within the cells from **6 d** and **7 d** correspondingly. This reaction cannot be triggered by H_2O_2 (compare B and C in Figure 6), but by some other oxidant.

Based on the reactivity of **3 d** and **7 d** in cell free settings (Figure 5), we assume that this oxidant can be an intracellular peroxidase or the oxidant with the "peroxidase-like" activity, for example Fe^{2+}/H_2O_2. A2780 and BL-2 cells loaded with type A agent **6 a** are stronger fluorescent than those loaded with type B agents **6 d** and **7 d** (Figure 6D, E). This indicates that **6 a** forms the higher amount of ferrocenium species in cells than **6 d** and **7 d** that is in agreement with properties of type A and B agents in cell free settings discussed above (Figure 5C, D, E).

To find out whether the ferrocenium species derived from **3 d** are important for the anticancer activity of this agent, we prepared its analogue brominated at the ferrocenyl fragment **3 d**_Br (Figure 1A). The redox potential of **3 d**_Br ($E_{1/2}$, *versus* FcH/FcH$^+$) is 116 mV, which is by 151 mV higher than the redox potential of **3 d**. These data indicate that **3 d**_Br is more resistant towards oxidation than **3 d**. Therefore, we could expect that in cells **3 d**_Br will form the lower amount of the ferrocenium species than **3 d**. We observed that after 2 h incubation with A2780 cells **3 d**_Br produce similar amount of tROS, but less mROS than **3 d** ($p < 0.05$, Student's t test). However, the effects of **3 d**_Br and **3 d** on the level of mROS at 4 h incubation were found to be the same. Further, we observed that cytotoxicity of **3 d**_Br and **3 d** towards A2780 and CLL cells are identical (Table 1, Figure 2C). Assuming that **3 d**_Br and **3 d** act via the same mechanism, these results allow concluding that the reduced form (**3 d**) rather than the oxidized one (**3 d**) are responsible for ROS-generating and anticancer properties of drug **3 d**.

Cancer cell specificity of agent 3 d

We investigated cancer cell specificity of **3 d** in two experiments. First, by using fluorescence microscopy we compared the mROS level in representative cancer (human ovarian A2780 cells) and normal cells (human SBLF9 fibroblasts). These cells were loaded with **3 d**, incubated for 2 h, washed, loaded with MitoSOX^{TM} probe (mROS probe) and imaged. We observed the increased level of mROS in the cancer cells, but not in the normal cells (Figures 3D–O).

In the latter experiment we compared cancer and normal cells of different origins: human ovarian carcinoma *versus* human primary fibroblasts. Therefore, the effect observed is not necessarily caused by differences in cancer *versus* normal cellular phenotype. To address this issue, we compared anticancer effects of **3 d** towards cancer and normal cells originated from blood. They included chronic lymphocytic leukemia (CLL), B- and T-cells. We found that drug **3 d** kills both CLL and B-cells with similar efficacy, whereas it is substantially less toxic towards T-cells. These data indicate that **3 d** is not fully cancer cell specific. It can affect at least some normal cells thereby leading to the undesired toxicity.

Antitumor effects of 3 d

We evaluated the anticancer activity of **3 d** in C57/BL6N mice carrying Nemeth-Kellner lymphoma (NK/Ly). The agent was formulated in cremophore/ethanol/saline (1/1/4, v/v/v) mixture. As a negative control we injected the mice with the carrier only. Furthermore, **3 a** formulated in the same carrier was used as a positive control. The agents and the carrier were applied at the dose of 8 mg/kg during the course of 10 injections, done every second day. The first injection was done one day after the tumor inoculation. On day 34, when the tumor weight in the carrier group was approaching 15% of initial animal weight, all animals were sacrificed, tumors were removed, weighted and fixed (Figure 7A). We observed that the average tumor weight in the **3 a** group was lower than that in the carrier group ($p < 0.05$, Mann-Whitney test). In contrast, **3 d** did not reduce the

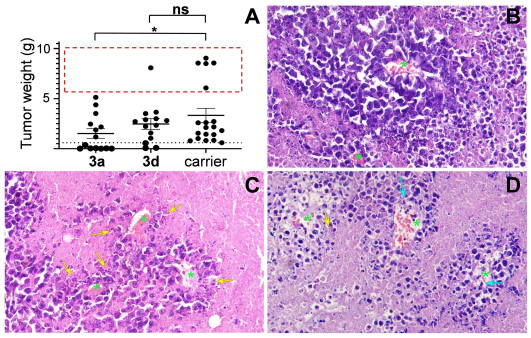

Figure 7. A: Tumor weigh in the studied groups at the end of the experiment. Statistic parameters were calculated by Mann-Whitney test. Dotted black line demonstrate the weight limit of 0.6 g, below which abundant granulomatous tissue was found in tumors. The area of large tumors is indicated with dotted red square. **B–D**: Histological analysis of selected tumors demonstrating blood vessels located deep inside tumor masses in the carrier (inset **B**), type A agent **3 a** (**C**) and type B agent **3 d** (**D**) groups. Blood vessels are indicated with green asterisks. Cell decay is indicated with yellow arrows. Tumor cells entering blood vessels space are shown with blue arrows. Anucleated areas are necrotic. H&E staining, 40×0.75 high-NA objective.

average tumor weight as compared to the carrier group. Under our experimental settings we observed that tumors grow heterogeneously in the carrier group. Therefore, only strong antitumor effects will be apparent at the end point measurement averaged over all animals. We observed that **3d** prevents the growth of large tumors (>5.2 g, dotted red square area in Figure 7A). In particular, only one animal with such a large tumor was present in the **3d** group (7%, N=14). In the positive control **3a** group no such animals were detected (0%, N=14), whereas the carrier group had 5 such animals (26%, N=19). We also found that tumors with masses <0.6 g consist mostly of granulomatous tissue formed around necrotic tumor masses (regressing tumors). All other tumors were identified as progressing tumors. At the end of the in vivo experiment 3 animals in the **3d** group (21%), 7 animals in the **3a** group (50%) and no animals in the carrier group (0%) had regressing tumors (Figure S3, Supporting Information).

Histological analysis of tumor samples demonstrated that in all groups tumors are highly vascularized, covered by the distinct border of connective tissue surrounded by granulomatous tissue. Especially strong difference between the groups is observed close to the blood vessels indicated with green asterisks in Figure 7B–D. They are surrounded by the abundant number of growing tumor cells in the carrier group (Figure 7B). An abundant tumor death (blue arrows), formation of picnotic nuclei, apoptotic debris and subsequent necrotic areas (pink color) were observed in the **3a** group (Figure 7C). Furthermore, no tumor cells were observed in vessel spaces making a general impression of the strong toxic action of the compounds coming from deep supplying vessels inside the tumors. In the **3d** group in the area of blood vessels the tumor growth is much less abundant than in the carrier group and some dying cells (blue arrows) are observed. Additional dying tumor cells in other areas are also observed (yellow arrows) (Figure 7C). Thus, **3d** exhibits the moderate anticancer effect in vivo, which is however weaker than that of positive control **3a** at the selected conditions.

Conclusion

By the optimization the chemical structure of type B aminoferrocene-based agent **1c** we could substantially improve its anticancer efficacy towards human ovarian cancer A2780 cells from IC_{50} 46.1±8.5 μM for **1c** to 7.0±1.3 μM for the optimized agent **3d**. We found that **3d** is cytotoxic also towards other cells (Burkitt's lymphoma BL-2 cell line and primary chronic lymphocytic leukemia CLL cells) in the low μMolar range. The anticancer efficacies of **3d** and the best known type A agent **3a** in vitro are comparable. **3d** exhibits significant toxicity towards B-cells, whereas it does not affect T-cells and SBLF9 fibroblasts. Agents **3d** and **3a** acts differently from each other. In particular, the uptake of **3d** occurs via the passive mechanism, whereas the uptake of **3a** is energy dependent. **3d** induces production of mitochondrial ROS (mROS), whereas **3a** generates total ROS and no mROS. Agent **3d** does not generate ROS directly as **3a** does, but rather acts indirectly by reducing the mitochondrial membrane potential. By using the fluorogenic version of **3d**, we observed that it is partially oxidized in cells with formation of ferrocenium species. However, an analogue **3d**_Br, which has substantially higher redox potential than **3d** (+151 mV), was found to have the same anticancer efficacy as **3d**. These data indicated that the neutral form of the drug is responsible for its anticancer properties. Finally, we found that **3d** exhibits moderate anticancer activity in vivo against murine Nemeth-Kellner lymphoma in C57/BL6N mice. Thus, this is the only AF-based agent, acting by increasing the level of intracellular mROS, which is applicable in vivo. All other known agents either exhibit low activity[11] or are too toxic.[10]

Experimental Section

All experimental data, synthesis and assay protocols are provided in Supporting Information.

Acknowledgements

We thank German Research Council (DFG, grant 1418/7-2) and the European Union's Horizon 2020 research and an innovation program FET Open (grant agreement No 861878, project "NeutroCure") for funding as well as Dr. Volodymyr Vovk and Halyna Sosna, Lviv, Ukraine for their help pathohistological analysis. Tissue imaging was done using infrastructure established under National Research Foundation of Ukraine grant 2020.02.0131. Open Access funding enabled and organized by Projekt DEAL.

Conflict of Interest

The authors declare no conflict of interest.

Data Availability Statement

The data that support the findings of this study are available in the supplementary material of this article.

Keywords: anticancer drugs · ferrocene · mitochondrion · reactive oxygen species

[1] a) B. Perillo, M. Di Donato, A. Pezone, E. Di Zazzo, P. Giovannelli, G. Galasso, G. Castoria, A. Migliaccio, *Exp. Mol. Med.* **2020**, *52*, 192–203; b) C. R. Reczek, N. S. Chandel, *Ann. Rev. Cancer Biol.* **2017**, *1*, 79–98.
[2] a) S. Daum, V. Chekhun, I. Todor, N. Lukianova, Y. Shvets, L. Sellner, K. Putzker, J. Lewis, T. Zenz, I. A. de Graaf, G. M. Groothuis, A. Casini, O. Zozulia, F. Hampel, A. Mokhir, *J. Med. Chem.* **2015**, *58*, 2015–2024; b) M. Schikora, A. Reznikov, L. Chaykovskaya, O. Sachinska, L. Polyakova, A. Mokhir, *Bioorg. Med. Chem. Lett.* **2015**, *25*, 3447–3450; c) P. Marzenell, H. Hagen, L. Sellner, T. Zenz, R. Grinyte, V. Pavlov, S. Daum, A. Mokhir, *J. Med. Chem.* **2013**, *56*, 6935–6944; d) H. Hagen, P. Marzenell, E. Jentzsch, F. Wenz, M. R. Veldwijk, A. Mokhir, *J. Med. Chem.* **2012**, *55*, 924–934.
[3] M. F. Renschler, *Eur. J. Cancer* **2004**, *40*, 1934–1940.
[4] G. Jaouen, A. Vessières, S. Top, *Chem. Soc. Rev.* **2015**, *44*, 8802–8817.

[5] M. Doering, L. A. Ba, N. Lilienthal, C. Nicco, C. Scherer, M. Abbas, A. A. Peer Zada, R. Coriat, T. Burkholz, L. Wessjohann, M. Diederich, F. Batteux, M. Herling, C. Jacob, *J. Med. Chem.* **2010**, *53*, 6954–6963.
[6] S. Daum, S. Babiy, H. Konovalova, W. Hofer, A. Shtemenko, N. Shtemenko, C. Janko, C. Alexiou, A. Mokhir, *J. Inorg. Biochem.* **2017**, *178*, 9–17.
[7] S. Daum, V. Reshetnikov, M. Sisa, T. Dumych, M. D. Lootsik, R. Bilyy, E. Bila, C. Janko, C. Alexiou, M. Herrmann, L. Sellner, A. Mokhir, *Angew. Chem. Int. Ed.* **2017**, *56*, 15545–15549; *Angew. Chem.* **2017**, *129*, 15751–15755.
[8] a) W. H. Koppenol, P. L. Bounds, C. V. Dang, *Nat. Rev. Cancer* **2011**, *11*, 325–337; b) O. Warburg, *Science* **1956**, *123*, 309–314.
[9] M. G. Vander Heiden, R. J. DeBerardinis, *Cell* **2017**, *168*, 657–669.
[10] V. Reshetnikov, H. G. Özkan, S. Daum, C. Janko, C. Alexiou, C. Sauer, M. R. Heinrich, A. Mokhir, *Molecules* **2020**, *25*, 2545.
[11] V. Reshetnikov, S. Daum, C. Janko, W. Karawacka, R. Tietze, C. Alexiou, S. Paryzhak, T. Dumych, R. Bilyy, P. Tripal, B. Schmid, R. Palmisano, A. Mokhir, *Angew. Chem. Int. Ed.* **2018**, *57*, 11943–11946; *Angew. Chem.* **2018**, *130*, 12119–12122.
[12] H.-G. Xu, M. Schikora, M. Sisa, S. Daum, I. Klemt, C. Janko, C. Alexiou, G. Bila, R. Bilyy, W. Gong, M. Schmitt, L. Sellner, A. Mokhir, *Angew. Chem. Int. Ed.* **2021**, *60*, 11158–11162; *Angew. Chem.* **2021**, *133*, 11258–11262.
[13] a) S. S. Sabharwal, P. T. Schumacker, *Nat. Rev. Cancer* **2014**, *14*, 709–721; b) L. Ippolito, E. Giannoni, P. Chiarugi, M. Parri, *Front. Immunol.* **2020**, *10*, 256, 10.3389/fonc.2020.00256.
[14] S. Daum, J. Toms, V. Reshetnikov, H. G. Özkan, F. Hampel, S. Maschauer, A. Hakimioun, F. Beierlein, L. Sellner, M. Schmitt, O. Prante, A. Mokhir, *Bioconjugate Chem.* **2019**, *30*, 1077–1086.
[15] a) A. Paul, R. Borrelli, H. Bouyanfif, S. Gottis, F. Sauvage, *ACS Omega* **2019**, *4*, 14780–14789; b) S. D. Waniek, J. Klett, C. Förster, K. Heinze, *Beilstein J. Org. Chem.* **2018**, *14*, 1004–1015.

Manuscript received: December 10, 2021
Version of record online: April 13, 2022